Open

CX$_3$CR1$^+$ macrophages support IL-22 production by innate lymphoid cells during infection with *Citrobacter rodentium*

C Manta[1], E Heupel[2], K Radulovic[1], V Rossini[1], N Garbi[3], CU Riedel[2] and JH Niess[1]

Innate immune cells, such as intestinal epithelial cells, dendritic cells (DCs), macrophages, granulocytes, and innate lymphoid cells provide a first line of defence to enteric pathogens. To study the role of CX$_3$CR1$^+$ DCs and macrophages in host defence, we infected CX$_3$CR1-GFP animals with *Citrobacter rodentium*. When transgenic CX$_3$CR1-GFP animals are infected with the natural mouse pathogen *C. rodentium*, CX$_3$CR1$^{-/-}$ animals showed a delayed clearance of *C. rodentium* as compared with (age- and sex-matched) wild-type B6 animals. The delayed clearance of *C. rodentium* is associated with reduced interleukin (IL)-22 expression. In *C. rodentium*-infected CX$_3$CR1-GFP animals, IL-22 producing lymphoid-tissue inducer cells (LTi cells) were selectively reduced in the absence of CX$_3$CR1. The reduced IL-22 expression correlates with decreased expression of the antimicrobial peptides RegIIIβ and RegIIIγ. The depletion of CX$_3$CR1$^+$ cells by diphtheria toxin injection in CX$_3$CR1-GFP×CD11c.DOG animals confirmed the role of CX$_3$CR1$^+$ phagocytes in establishing IL-22 production, supporting the clearance of a *C. rodentium* infection.

INTRODUCTION

Innate immune cells, such as intestinal epithelial cells, dendritic cells (DCs), macrophages, granulocytes, and innate lymphoid cells (ILC) provide a first line of defence to insults in the gut, which is exposed to a complex intestinal microflora and, occasionally, pathogens.[1] Defective immune responses to the commensal microflora may mediate intestinal diseases such as Crohn's disease and ulcerative colitis.[2] Infiltration of DCs and macrophages is a characteristic of intestinal inflammation.[3] The majority of F4/80$^{(high)}$ CX$_3$CR1$^+$ macrophages produce interleukin (IL)-10 in a CX$_3$CR1-dependent manner in the steady state,[4] whereas a small population of F4/80$^{(low)}$ CX$_3$CR1$^+$ DCs secrete IL-12, IL-23, and tumor necrosis factor (TNF)-α, and are able to activate T cells.[5–7] CX$_3$CR1 has been implicated in host defence to *Salmonella* and bacterial peritonitis,[8,9] but its role in host defence in the large intestine has not been studied in detail.

Citrobacter rodentium is a natural extracellular enteric mouse pathogen that serves as a mouse model of human infections with enteropathogenic *Escherichia coli*.[10] *C. rodentium* colonizes the cecum and colon of mice after infection.[11] *C. rodentium* targets and infects intestinal epithelial cells by characteristic attaching and effacing lesions.[12] It represents an excellent model system to study innate host immune responses in the gut.[13] Clearance of *C. rodentium* by the hosts partially depends on IL-22, a member of the extended IL-10 cytokine family, as shown in studies with IL-22$^{-/-}$ animals.[14] IL-22 induces expression of intestinal antimicrobial peptides (RegIIIβ and RegIIIγ, β-defensin-2, and β-defensin-3)[15] and facilitates host responses by modulating the expression of various chemokines, including CXCL1, CXCL5, and CXCL9.[16–18] IL-23 promotes IL-22 expression, as IL-23$^{-/-}$ animals succumb to *C. rodentium* infection.[19,20] IL-1β, the γc cytokines IL-2, IL-7, and IL-15, and lymphotoxin controls the production of IL-22 by related orphan receptor gamma-t (RORγt)$^+$ ILCs.[21] Several ILCs have been recently described that are characterized by signature cytokines.[22] IL-22 production is a characteristic of ILC22 cells. These cells share characteristics of lymphoid tissue inducer (LTi) and natural killer (NK) cells. ILC17 and LTi cells both produce IL-17A and IL-22.[22] All ILC share an Id2-dependent precursor cell for their development.[22] ILC22, ILC17, and LTi all express the transcription factor RORγt.

DCs and macrophages have been suggested to support the production of IL-22 by ILCs.[23] DCs support IL-22 production by ILCs in a lymphotoxin-dependent pathway.[24] In addition, DC-derived IL-23 and macrophage-derived IL-1β facilitates IL-22 production by ILCs.[19] Addition of IL-25 to cultures of IL-17BR^{+} CD11c^{+} DCs/macrophages is able to suppress IL-22 production by RORγt^{+} ILCs.[25] In addition, Toll-like receptor agonists were shown to induce IL-22 expression by ILCs *in vitro* via stimulation of DCs and macrophages.[21] However, the subset of DC or macrophages promoting ILC IL-22 expression is not yet identified.

Given the high abundance of CX_3CR1^+ cells in the colonic lamina propria (cLP), we hypothesized that CX_3CR1^+ phagocytes may have a role in regulating IL-22 production by ILCs in response to intestinal bacterial pathogens, and thus be critical for protection. Using a murine model of innate-mediated
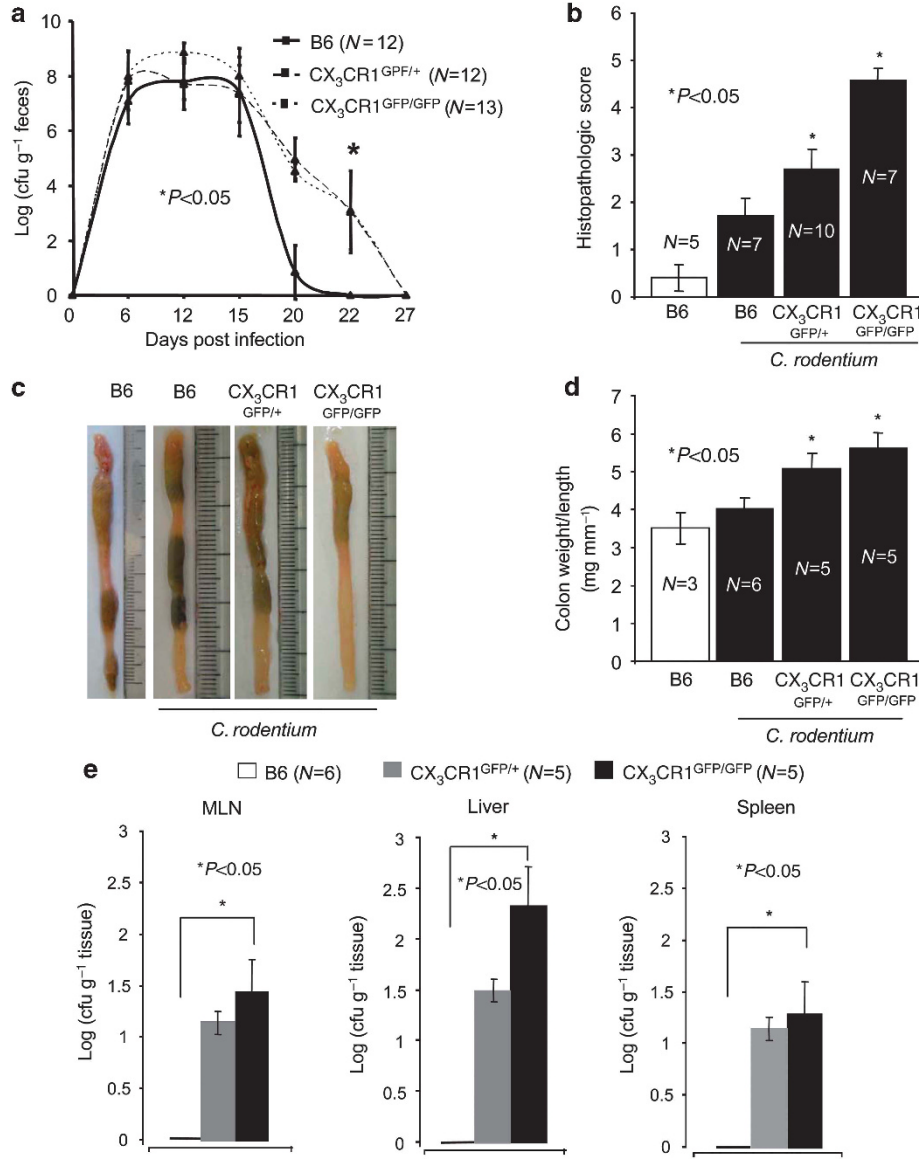

Figure 1 Delayed clearance of *Citrobacter rodentium* in CX_3CR1-GFP animals. (**a**) *C. rodentium* counts in fecal samples from wt B6 animals and (age- and sex-matched) heterozygous and homozygous CX_3CR1-GFP animals were determined by collecting fecal pellets from each animal every 2–3 days over the course of the infection. Pellets were weighted and resuspended in 1 ml of phosphate-buffered saline (PBS), plated in serial dilutions, and bacterial load was calculated as cfu g^{-1} feces. *P*-values were calculated with a nonparametric Student's *t*-test; $P<0.05$ was considered statistically significant. (**b**) Histopathological scores of colon sections taken from control or infected B6, $CX_3CR1^{GFP/+}$, and $CX_3CR1^{GFP/GFP}$. In the nonparametric Student's *t*-test, $P<0.05$ was considered statistically significant. (**c**) At the end of the experiment, colons were removed and representative colons of the indicated groups are shown. (**d**) The colon weight and length was determined and expressed as colon weight/length ratios. In the nonparametric Student's *t*-test, $P<0.05$ was considered statistically significant. (**e**) Colony-forming units (CFU) from plates spotted with homogenates from liver, spleen, and mesenteric lymph nodes (MLN) of the indicated groups were determined. The numbers of animals per group of each experiment is given within the figure. In the nonparametric Student's *t*-test, $P<0.05$ was considered statistically significant.

protection against *C. rodentium*, we show that clearance of *C. rodentium* is delayed in the absence of CX_3CR1. CX_3CR1-GFP animals on a recombination-activating gene (RAG)$^{-/-}$ background are highly susceptible to *C. rodentium* infection. Absence of CX_3CR1 resulted in reduced IL-22 expression and reduced numbers of $CD3^-CD4^+ROR\gamma t^+CD127^+CD117^+$ ILC cells. In addition, depletion of $CX_3CR1^+CD11c^+$ cells further indicated a role of $CX_3CR1^+CD11c^+$ macrophages in facilitating IL-22 production, supporting host defence against *C. rodentium* infection.

RESULTS

Delayed *C. rodentium* clearance in absence of CX_3CR1 in $CX_3CR1^{GFP/GFP}$ animals

The fractalkine receptor CX_3CR1 is required for the clearance of *Salmonella* in the small intestine[8,26] and in a peritoneal sepsis model,[9] although the cellular and molecular mechanisms are not yet fully understood. Increased susceptibility of $CX_3CR1^{GFP/GFP}$ animals, in which the green fluorescent protein (GFP) is inserted into two alleles of the *CX_3CR1* locus and are hence CX_3CR1-deficient, to *Salmonella* can be in part
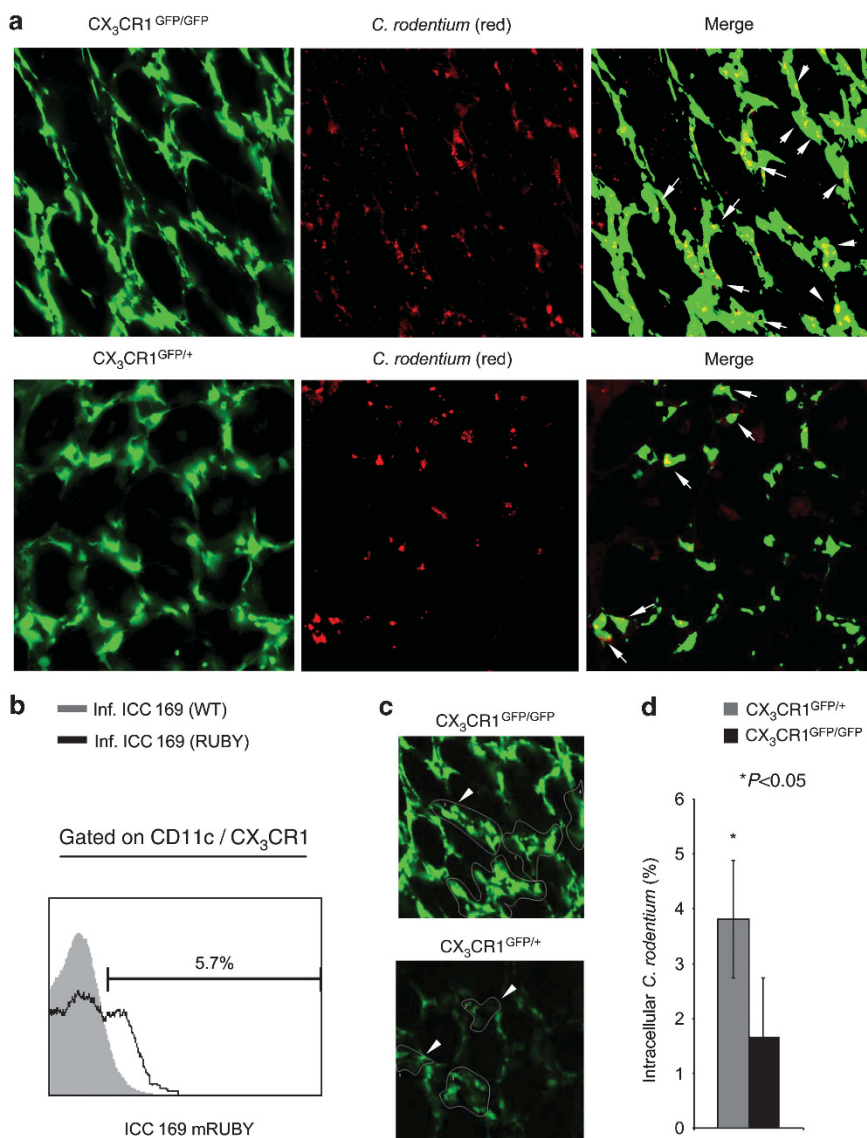
Figure 2 *Citrobacter rodentium* can be located in CX_3CR1^+ macrophages. (**a**) Homozygous CX_3CR1-GFP animals were infected with *C. rodentium* mutants expressing the red fluorescent protein mRuby. Twelve days post infection, living intestinal tissues from the proximal colon was analyzed by *ex vivo* microscopy. (**b**) $CX_3CR1^+CD11c^+$ cells were isolated from homozygous CX_3CR1-GFP animals infected with the *C. rodentium* mutant ICC 169 expressing the red fluorescent protein mRuby. Colonic lamina propria isolates were stained for CD11c and analyzed by flow cytometry. Histograms were obtained by gating on CX_3CR1-GFP$^+CD11c^+$ cells. Gray areas represent isolates obtained from animals infected with *C. rodentium* ICC 169; open histograms represent isolates obtained from animals infected with mRuby expressing *C. rodentium* mutants. (**c**) CX_3CR1^+ cells were defined as area of interest and scatter diagrams obtained. The percentage of *C. rodentium* located in CX_3CR1^+ macrophages was determined. (**d**) Mean (±s.e.m.) percentage of *C. rodentium* located in CX_3CR1^+ macrophages from the indicated mice is shown. *P*-values were calculated with a nonparametric Student's *t*-test; $P < 0.05$ was considered statistically significant.

explained by the reduced production of TNF-α, interferon-γ, IL-6, and inducible nitric oxide synthase.[9] The infection of B6 and $CX_3CR1^{GFP/+}$, and $CX_3CR1^{GFP/GFP}$ animals with *C. rodentium* is associated with an increased colonic fractalkine (CX_3CL1, the ligand of CX_3CR1) expression at day 12 and 20 post infection (p.i.; **Supplementary Figure S1** online). To determine the contribution of CX_3CR1 to host defence to *C. rodentium*, we infected wild-type (wt, littermate controls) heterozygous $CX_3CR1^{GFP/+}$ and homozygous $CX_3CR1^{GFP/GFP}$ animals[27] by oral gavage, and monitored the number of pathogenic bacteria in the feces for 27 days. In wt B6 animals *C. rodentium* burden in feces peaked between day 10–15, declined over time, and was not detectable at day 21, consistent with previous work from our group (**Figure 1a**).[11] Although the initial kinetics were comparable to control mice, *C. rodentium* burden in feces of $CX_3CR1^{GFP/+}$ and $CX_3CR1^{GFP/GFP}$ animals remained >2 logs higher than in age- and sex-matched B6 animals on days 20 and 22 p.i., and complete *C. rodentium* clearance was delayed until day 27 p.i. for about 1 week (**Figure 1a**). The delayed clearance of *C. rodentium* in $CX_3CR1^{GFP/+}$ and $CX_3CR1^{GFP/GFP}$ animals is associated with increased histopathological and macroscopic signs of *C. rodentium*-induced colitis (**Figure 1b** and **c**), increased colon weight/length ratios (**Figure 1d**), and reduced anti-*C. rodentium* immunoglobulin G (IgG) titers (**Supplementary Figure S2** online). *C. rodentium* could not be detected in homogenates of mesenteric lymph nodes (MLNs), liver, and spleen of B6 animals, confirming previous reports (**Figure 1e**). By contrast, on day 12 p.i., *C. rodentium* could be cultured from homogenates of MLNs, liver, and spleen of $CX_3CR1^{GFP/+}$ and $CX_3CR1^{GFP/GFP}$ animals (**Figure 1e**). *C. rodentium* counts were higher in $CX_3CR1^{GFP/GFP}$ animals compared with $CX_3CR1^{GFP/+}$ animals in all organs tested, but this effect was not statistically significant. Thus, *C. rodentium* translocates across the intestinal epithelium to MLN and liver if CX_3CR1 levels are reduced or absent. Overall, these data indicated that CX_3CR1 is involved in the clearance of the *C. rodentium* infection, and deficiency in CX_3CR1 is associated with a significant increase in the severity of the *C. rodentium* infection.

C. rodentium localizes within CX₃CR1⁺ phagocytes

The *C. rodentium* infection is associated with an infiltration of CX_3CR1^+ cells (**Supplementary Figure S3** online). Significant differences between heterozygous and homozygous CX_3CR1-GFP animals were not observed (**Supplementary Figure S3E** and **F** online). Multi-color flow cytometry demonstrated that $F4/80^+CD11c^+$ macrophages and $F4/80^{(low)}CD11c^+$ DCs expressed CX_3CR1 (**Supplementary Figure S3B** and **C** online). In *C. rodentium*-infected animals, an increase of the $CX_3CR1^+F4/80^+CD11c^+$ macrophages was observed (**Supplementary Figure S3B** online). To examine *C. rodentium* infections in $CX_3CR1^{GFP/+}$ and $CX_3CR1^{GFP/GFP}$ by fluorescence microscopy, we generated a red fluorescent *C. rodentium* strain (RF-*C. rodentium*) constitutively expressing the protein mRuby from a single copy of a derivative of plasmid p16S*lux*[28] integrated into the bacterial chromosome (**Supplementary Figure S4** online). Intestinal tissues of infected animals were analyzed by *ex vivo* confocal imaging 12 days p.i. (peak infection). RF-*C. rodentium* had translocated into the cLP of the colon at peak infection (**Figure 2a**). RF-*C. rodentium* is closely associated with CX_3CR1^+ cells and can be located within CX_3CR1^+ cells (**Figure 2a**). RF-*C. rodentium* seems thus to be phagocytosed by CX_3CR1^+ macrophages in the cLP. Flow cytometry confirmed the presence of RF-*C. rodentium* within CX_3CR1^+ cells (**Figure 2b**). To further analyze the percentage of RF-*C. rodentium* located within CX_3CR1^+ DCs and macrophages in heterozygous and homozygous CX_3CR1-GFP animals, CX_3CR1^+ cells were defined as a region, for which colocalization of red and green fluorescent signals were analyzed by generating scatter diagrams (**Figure 2c** and **d**). In $CX_3CR1^{GFP/+}$ and $CX_3CR1^{GFP/GFP}$ animals, *C. rodentium* is found within the

Figure 3 Interleukin (IL)-22 expression is reduced in *Citrobacter rodentium*-infected $CX_3CR1^{GFP/GFP}$ animals. (**a**) From the proximal colon of noninfected and *C. rodentium*-infected $CX_3CR1^{GFP/GFP}$ and wild-type littermate controls mRNA was isolated. cDNA was prepared by reverse transcription and quantitative real-time PCR was performed with cyber green and the indicated primers. β-*actin* was used as a housekeeping gene to normalize cDNA input between samples. Normalized ct-values of the untreated samples (baseline) are set to 1 and values are plotted as fold expression of the baseline. The assays were carried out in triplicates. As per indicated, group 4 animals were analyzed. (**b**) IL-22 expression by colonic lamina propria (cLP) cell isolates from noninfected and *C. rodentium*-infected B6, (age- and sex-matched) and $CX_3CR1^{GFP/+}$ and $CX_3CR1^{GFP/GFP}$ animals was analyzed by multicolor flow cytometry. Numbers indicate the percentage of IL-22-positive cells. (**c**) cLP IL22⁺ cells from noninfected and *C. rodentium*-infected B6, (age- and sex-matched), and $CX_3CR1^{GFP/+}$ and $CX_3CR1^{GFP/GFP}$ animals were stained for CD3ε and CD4. Numbers indicate the percentage of CD3ε⁺, CD3ε⁺CD4⁺, CD4⁺, and CD3ε⁻CD4⁻ cells within the IL-22⁺ cell population. Data from an individual representative mouse per group (of five to seven individual mice analyzed per group) are shown. (**d**) cLP IL22⁺ CD3ε⁻CD4⁺ cells were (intracellular) stained for related orphan receptor gamma-t (RORγt) or surface stained for CD25, CD127, and CD117, and analyzed by multi-color flow cytometry. Opened curves represent the respective negative controls. Seven mice were analyzed and the data from a representative individual mouse are presented. Numbers represent the percentage of cells that are positive for the indicated antigen. (**e**) Mean (±s.e.m.) percentage of IL-22⁺ cells isolated from the cLP of *C. rodentium*-infected B6, (age- and sex-matched) and $CX_3CR1^{GFP/+}$ and $CX_3CR1^{GFP/GFP}$ animals is shown. In the nonparametric Student's *t*-test, $P < 0.05$ was considered statistically significant (*$P < 0.05$). (**f**) Mean (±s.e.m.) percentage of CD3ε⁻CD4⁺ lymphoid-tissue inducer cells within the IL-22⁺ cells from cLP isolates of B6, (age- and sex-matched) and heterozygous and homozygous CX_3CR1-GFP animals is shown. *P*-values were calculated with a nonparametric Student's *t*-test; $P < 0.05$ was considered statistically significant. (**g**) Total RNA isolated from the colonic tissues of noninfected and *C. rodentium*-infected B6, (age- and sex-matched), and $CX_3CR1^{GFP/+}$ and $CX_3CR1^{GFP/GFP}$ animals were reverse transcribed to cDNA and RegIIIγ, and (**h**) RegIIIβ expression was analyzed by qRT-PCR. The number of animals per group of each experiment is given within the figure. In the nonparametric Student's *t*-test, $P < 0.05$ was considered statistically significant.

CX_3CR1^+ macrophages/DC at peak infection. CX_3CR1 seems to somewhat increase the uptake of *C. rodentium* (4.8 vs. 1.6%). Hence, *C. rodentium* is phagocytosed by CX_3CR1^+ cells at peak infection.

## Absence of CX_3CR1 is associated with reduced IL-22 expression

As IL-22 has an important role for the clearance of the *C. rodentium* infection,[29] we screened B6 and heterozygous and homozygous CX_3CR1-GFP animals for IL-22 expression. IL-22 mRNA expression was first determined by quantitative

real-time PCR. IL-22 mRNA expression levels peaked at early infection (day 8 p.i.) and declined in the further course of the infection. Previous reports have already indicated that highest IL-22 expression can be found at early infection.[29,30] Infected $CX_3CR1^{GFP/GFP}$ animals produced significant less IL-22 mRNA as compared with littermate controls (**Figure 3a**). IL-22 expression was > 4-fold increased in *C. rodentium*-infected B6 mice at peak infection compared with noninfected controls. Significant differences between noninfected B6 and (age- and sex-matched) heterozygous and homozygous CX_3CR1-GFP animals were not observed (**Figure 3b**). In contrast, *C. rodentium*-infected
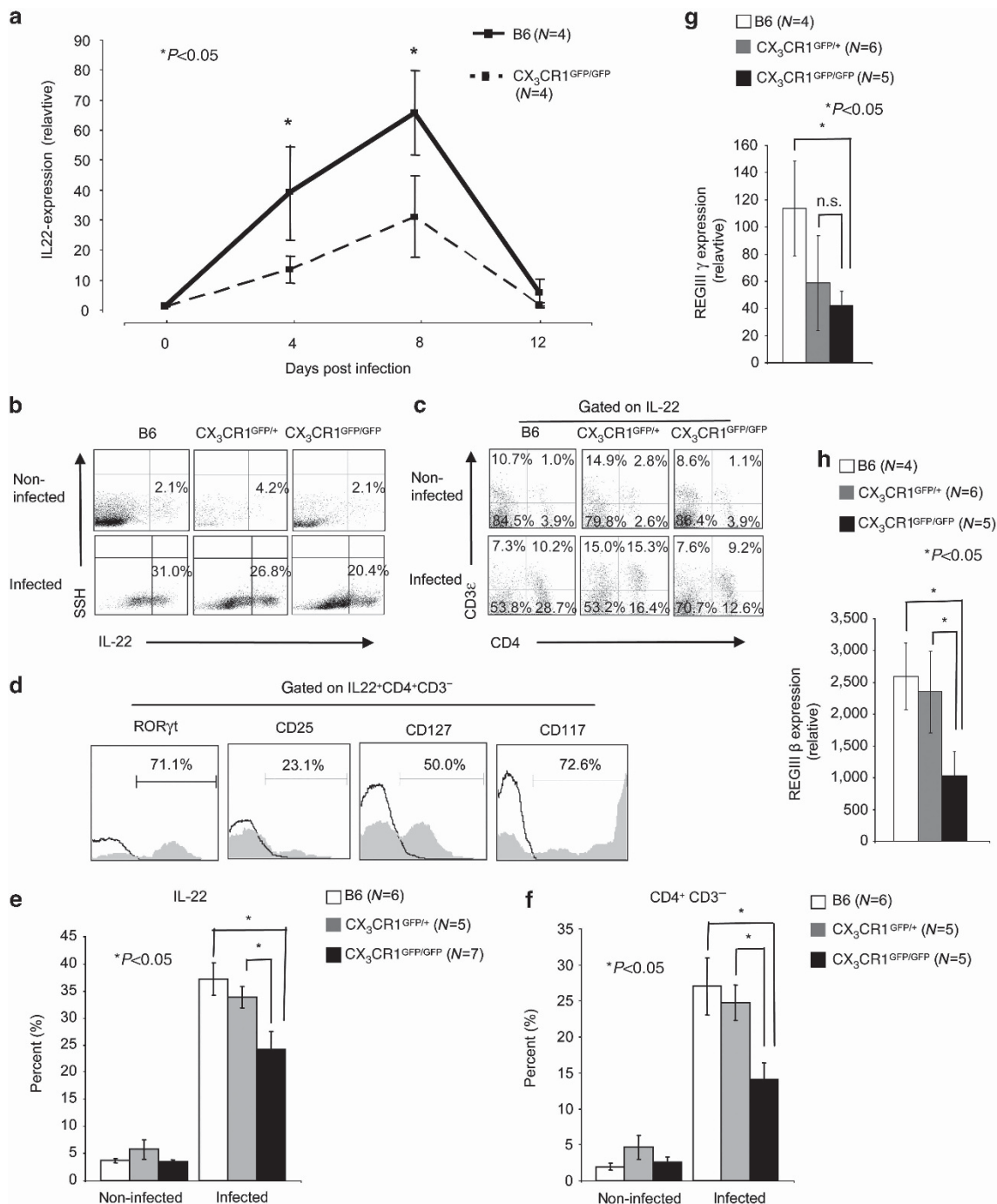
$CX_3CR1^{GFP/GFP}$ produced less IL-22 as compared with B6 animals (**Figure 3b** and **e**). At peak infection, differences in IL-10 production were not observed between heterozygous and homozygous CX_3CR1-GFP animals (data not shown), but IL-1β, IL12p40, and not IL-12p19 transcripts were reduced in these animals as compared with the B6 control mice (**Supplementary Figure S5** online). Our results show that normal CX_3CR1 expression is required for optimal colonic
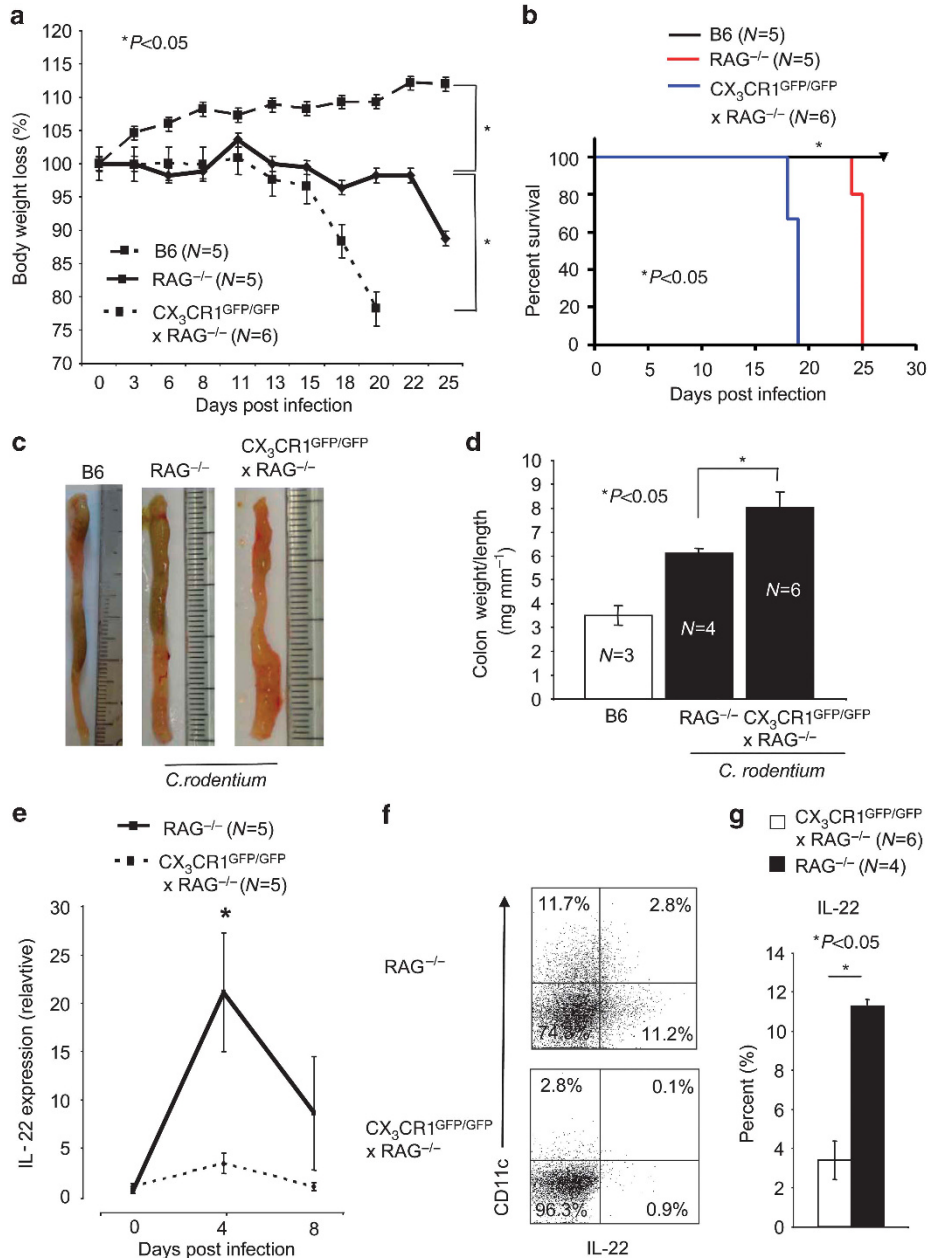
Figure 4 Recombination-activating gene (RAG)$^{-/-}$ mice lacking CX_3CR1 develop a rapid *Citrobacter rodentium* infection. (**a**) RAG$^{-/-}$×$CX_3CR1^{GFP/GFP}$ and RAG$^{-/-}$ mice were infected with $2×10^9$ *C. rodentium*. Mean±s.e.m. loss of body weight (%) per group is shown for the indicated animals. *P*-values were calculated with a nonparametric Student's *t*-test; *P*<0.05 was considered statistically significant. (**b**) Survival of RAG$^{-/-}$×$CX_3CR1^{GFP/GFP}$ and RAG$^{-/-}$ infected with $2×10^9$ *C. rodentium* is shown. (**c**) Colons were removed at the end of the experiment and representative colons of the indicated groups are shown. (**d**) The colon weight and length was determined and expressed as colon weight/length ratios. In the nonparametric Student's *t*-test, *P*<0.05 was considered statistically significant. (**e**) Interleukin (IL)-22 expression in the proximal colon of infected RAG$^{-/-}$ and RAG$^{-/-}$×$CX_3CR1^{GFP/GFP}$ animals was analyzed by quantitative real-time PCR. β-*actin* was used as housekeeping gene to normalize cDNA input between samples. Normalized ct-values of the noninfected samples (baseline) are set to 1 and values are plotted as fold expression of the baseline (**f**) IL-22 expression by colonic lamina propria (cLP) cell isolates from *C. rodentium*-infected RAG$^{-/-}$, (age- and sex-matched) and RAG$^{-/-}$×$CX_3CR1^{GFP/GFP}$ animals was analyzed by multicolor flow cytometry. Numbers indicate the percentage of IL-22-positive cells. (**g**) Mean (±s.e.m.) percentage of IL-22$^+$ cells isolated from the cLP of *C. rodentium*-infected B6, (age- and sex-matched), and $CX_3CR1^{GFP/+}$ and $CX_3CR1^{GFP/GFP}$ animals is shown. In the nonparametric Student's *t*-test, *P*<0.05 was considered statistically significant (*P<0.05).

IL-22 production in infected animals (**Figure 3**). Several cell population in the colon produce IL-22, including Th17, γδ T cells, ILC17, ILC22, and LTi cells as major producers.[22] We carried out multi-color flow cytometry to investigate whether there was a specific cell population whose IL-22 production was particularly affected in mice with reduced CX_3CR1 expression. For this, cLP cell isolates from noninfected and *C. rodentium*-infected B6, heterozygous, and homozygous CX_3CR1-GFP animals were stained for IL-22, CD3ε, and CD4 (**Figure 3c**). In B6 mice, the population of $CD4^+CD3^-IL-22^+$ cells increased from about ~6% to over 20% upon infection with *C. rodentium* (**Figure 3c,f**). This population was significantly reduced in infected $CX_3CR1^{GFP/GFP}$ mice compared with B6 animals (**Figure 3e,f**). The $CD4^-CD3^-IL-22^+$ cells could be $CD4^-NKp46^+ROR\gamma t$ and $CD4^-NKp46^-ROR\gamma t$ ILCs.[25] Further analysis of the $CD4^+CD3^-IL-22^+$ population revealed that these cells are characterized by RORγt, CD25, CD127, and CD117 expression, indicating that $CD4^+CD3^-$ IL-22-producing ILCs are LTi cells (**Figure 3d**). The reduced IL-22 expression in *C. rodentium*-infected $CX_3CR1^{GFP/GFP}$ animals is associated with reduced RegIIIγ and RegIIIβ expression in the colon of infected $CX_3CR1^{GFP/GFP}$ mice (**Figure 3g,h**), two secreted lectins involved in defence to pathogens in the intestinal tract.[31] Our data indicated that reduced CX_3CR1 levels result in impaired IL-22 expression, specifically by $CD4^+CD3^-$ LTi cells in the colon of *C. rodentium*-infected animals, to a similar extent in CX_3CR1 heterozygous and knock-out mice. IL-22 has been shown to be critical for clearance of *C. rodentium*.[29] Thus, the reduced expression of IL-22 by colonic LTi in infected mice with reduced CX_3CR1 described here is a likely explanation of impaired *C. rodentium* clearance in these mice (**Figure 1**).

Accelerated lethality in $RAG^{-/-}$ mice lacking CX_3CR1

To investigate the specific defect of LTi cells without the contribution of T-lymphocyte-produced IL-22, we next analyzed *C. rodentium* infections in $RAG^{-/-}$ and $RAG^{-/-} \times CX_3CR1^{GFP/GFP}$ animals. We measured the body weight and collected fecal samples to determine the viable counts of *C. rodentium*. The experiment was ended when > 15% body weight loss occurred or when infected animals displayed serious signs of colitis such as rectal prolapses. Unlike wt B6 animals, $RAG^{-/-}$ animals did not clear the infection, confirming previous reports, and had to be killed by day 25 of infection (**Figure 4a,b**).[32] The absence of CX_3CR1 in $RAG^{-/-} \times CX_3CR1^{GFP/GFP}$ animals resulted in an accelerated body weight loss and lethality as compared with $RAG^{-/-}$ animals (**Figure 4a,b**). Also, *C. rodentium* infection in $RAG^{-/-} \times CX_3CR1^{GFP/GFP}$ is associated with increased macroscopic signs of *C. rodentium*-induced colitis (**Figure 4c**) and increased colon weight/colon length ratios (**Figure 4d**). Moreover, *C. rodentium* infection in $RAG^{-/-} \times CX_3CR1^{GFP/GFP}$ resulted in a strong reduction of IL-22-producing cells in the cLP. Reduced IL-22 mRNA expression was most evident at early infection (day 4 p. i.; **Figure 4e**). In addition, IL-22-expressing cells were reduced in $RAG^{-/-} \times CX_3CR1^{GFP/GFP}$ animals (**Figure 4f** and **g**). The CX_3CR1-dependent IL-22 production

by LTi cells promotes innate immunity to enteric pathogens in the large intestine.

Depletion of $CX_3CR1^+ CD11c^+$ cells result in severe pathology

As CX_3CR1 is expressed by macrophages/DCs and NK cells (**Supplementary Figure S3A** online), we crossed CX_3CR1-GFP animals with CD11c.DOG animals to further examine the role of $CX_3CR1^+ CD11c^+$ cells for the induction of IL-22 production by innate lymphocytes without the possible contribution of CX_3CR1^+ NK cells. Efficient depletion of $CD11c^+$ cells can be achieved by diphtheria toxin injection over prolonged times.[33] $CX_3CR1^+CD11c^+$ phagocytes can be depleted for more than 14 days as indicated by flow cytometry analysis of isolates obtained from spleen, MLN, and cLP (**Figure 5a**). Fluorescence microscopy confirmed the efficient depletion of $CX_3CR1^+CD11c^+$ in CX_3CR1-GFP×CD11c. DOG animals (**Figure 5b**). We infected CD11c.DOG, CD11c. DOG×$CX_3Cr1^{GFP/+}$, and CD11c.DOG×$CX_3CR1^{GFP/GFP}$ animals with *C. rodentium*. In infected CD11c.DOG, CD11c. DOG×$CX_3CR1^{GFP/+}$, and CD11c.DOG×$CX_3CR1^{GFP/GFP}$ animals, $CD11c^+$ cells were depleted by diphtheria toxin injection. The depletion of $CX_3CR1^+ CD11c^+$ cells resulted in an accelerated body weight loss (**Figure 5c**), increased lethality (**Figure 5d**), and increased *C. rodentium* load in MLN, spleen, and liver (**Figure 5h**). Significant differences between depleted CD11c.DOG, CD11c.DOG×$CX_3CR1^{GFP/+}$, and CD11c.DOG×$CX_3CR1^{GFP/GFP}$ animals were not observed (**Figure 5c, d** and **h**). Further analysis revealed that IL-22 expression is reduced after the depletion of $CX_3CR1^+CD11c^+$ phagocytes (**Figure 5e**). Multi-color flow cytometry demonstrated that the $CD4^+CD3^-IL-22^+$ innate cell population is reduced after the depletion of $CX_3CR1^+CD11c^+$ phagocytes (**Figure 5e–g**). $CX_3CR1^+CD11c^+$ DCs and macrophages hence seem to facilitate IL-22 production by ILCs during a *C. rodentium* infection.

DISCUSSION

In this study, we identified a role of CX_3CR1^+ phagocytes in clearance of a *C. rodentium* infection. Immunophenotyping by flow cytometry of $CX_3CR1^+CD11c^+$ cells demonstrated that CX_3CR1 is expressed by $F4/80^{(high)}CD11c^+$ and $F4/80^{(low)}CD11c^+$ cells in the cLP. $CX_3CR1^+CD11c^+$ cells encounter *C. rodentium* and support IL-22 production of ILCs in the cLP. In part, fractalkine/CX_3CL1 facilitates IL-22 production of ILCs by regulating IL-1β and IL-23p19 expression in *C. rodentium*-infected animals. Uptake of *C. rodentium* by CX_3CR1^+ cells may serve as a defence mechanism to enteric pathogen and initiate innate immune responses by supporting IL-22 production by ILCs (**Supplementary Figure S6** online).

We have not carried out our experiments with *C. rodentium* mutants lacking the structural components of a type III secretion system.[34] Hence, we cannot rule out that *C. rodentium* actively supports its uptake by CX_3CR1^+ cells. Experiments with fluorescent noninvasive commensal *E. coli* strain have demonstrated

that luminal bacteria are directly phagocytosed by CX_3CR1^+ macrophages residing beneath the epithelium in the cLP (data not shown). CX_3CR1^+ macrophages and DCs may hence serve as first sentinels after infection of the host with enteric pathogens and initiate rapid innate immune responses. Reduced IL-1β but not IL-23p19 transcripts were observed in infected $CX_3CR1^{GFP/GFP}$ animals in absence of CX_3CR1. We speculate that phagocytosed *C. rodentium* provide signals to CX_3CR1^+

phagocytes that help to facilitate IL-22 expression by ILCs. Reduced anti-*C. rodentium* IgG titers in $CX_3CR1^{GFP/GFP}$ animals indicated that CX_3CR1 (beside its effects on IL-22 expression) may also be involved in regulating adaptive immune responses required for the clearance of *C. rodentium*. Polymorphism of the *CX_3CR1* gene has been described to be associated with ileal Crohn's disease.[35] Our work indicates that the CX_3CR1–IL-22 axis could regulate REG IIIγ and REG IIIβ expression.
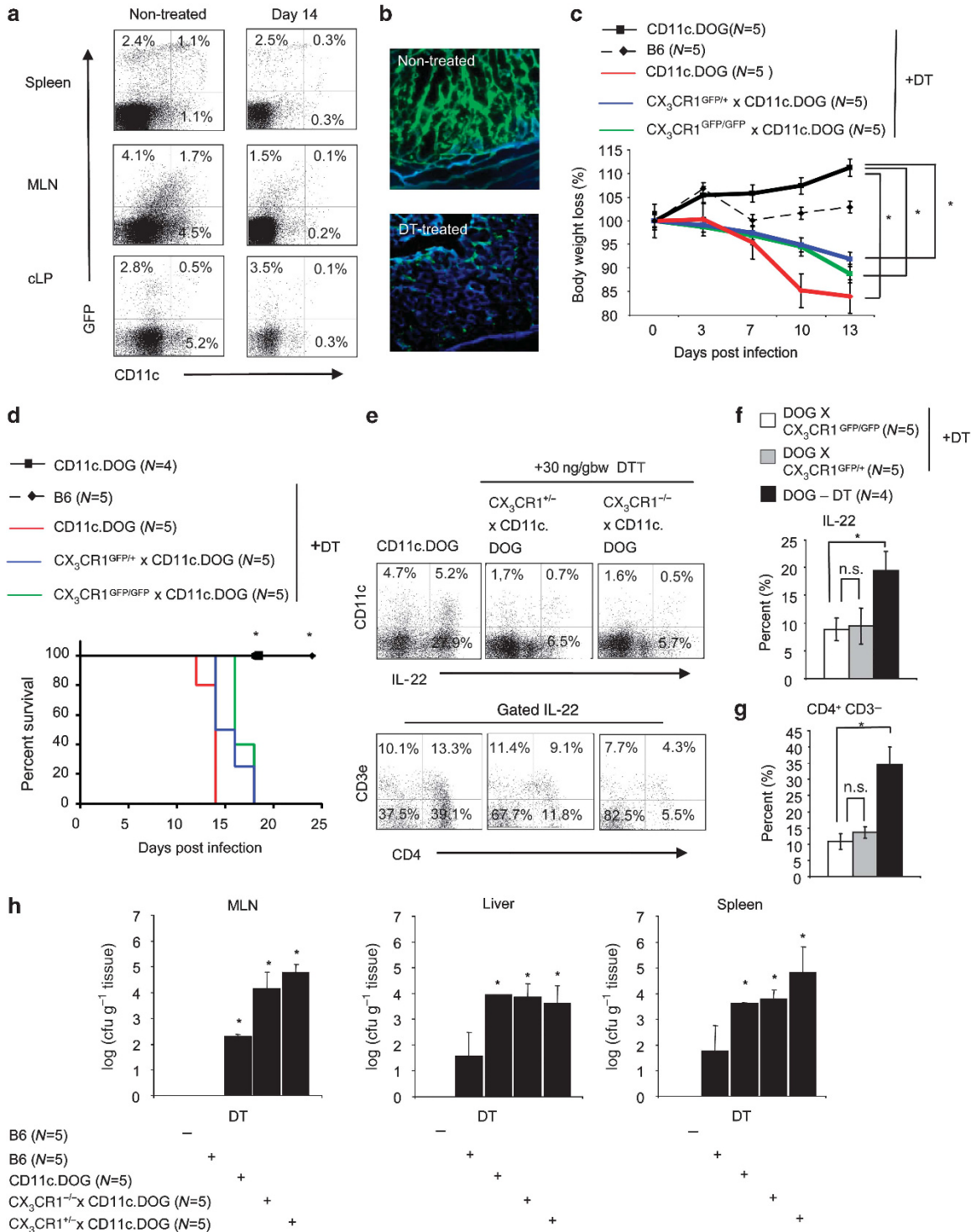
In addition, IL-22 has epithelial regenerative properties, increasing intestinal epithelial cell proliferation and wound healing, which also has a role in the protection of the host.[36,37] Malfunction of the CX_3CR1–IL-22 axis may thus contribute to the development of Crohn's disease.

The stimulation of isolated CX_3CR1^+ small intestine LP and cLP macrophages have dose-dependent effects on secretion of cytokines by macrophages.[38] Low concentration of CX_3CL1 decreased the production of TNF-α by lipopolysaccharide-stimulated macrophages.[38] High CX_3CL1 concentrations facilitate the production of pro-inflammatory cytokines, such as IL-23 and TNFα, in a peroxisome proliferator-activated receptor-γ-dependent mechanism.[38] In light of these observations, reduced IL-10 production by CX_3CR1^+ macrophages was observed in the steady state and tolerogenic conditions.[4] Bacterial peritonitis and/or injection of *Clostridium difficile* toxin A is associated with exacerbated disease in $CX_3CR1^{-/-}$ animals.[9,39] In part, the increased susceptibility of $CX_3CR1^{-/-}$ mice is mediated by impaired regulation of the heme oxygenase-1, TNF-α, IL-6, and inducible nitric oxide synthase production.[9,39] In spite of those findings, CX_3CR1 may provide environmental signals to macrophages that regulate their adaptation to microenviromental clues in the intestine.

As CX_3CR1 is expressed by DCs/macrophages and NK cells,[5,27,40–42] we crossed CX_3CR1-GFP animals with CD11c. DOG animals to further examine the role of $CX_3CR1^+CD11c^+$ cells for the induction of IL-22 production by innate lymphocytes without the possible contribution of CX_3CR1^+ NK cells. The depletion of $CD11c^+$ macrophages and DCs resulted in increased susceptibility of transgenic animals to the *C. rodentium* infection. The depletion of $CD11c^+CX_3CR1^+$ macrophages was associated with reduced IL-22 production and reduced numbers of $CD3^-CD4^+$ RORγt$^+$ LTi cells. The $CD11c^+$ cell depletion gives similar results in CD11c.DOG and CD11c. DOG×$CX_3CR1^{GFP/GFP}$ animals (that lack CX_3CR1). The lack of CX_3CR1 did not result to an additive effect after depletion

of $CD11c^+$ cells in infected animals. Thus, we would suggest a model in which CX_3CR1^+ macrophages in the gut supports IL-22 production by ILCs in infected animals required for the clearance of *C. rodentium*.

METHODS

Mice. Littermate C57BL/6J (B6) mice, CX_3CR1-GFP (B6.129P-$Cx_3cr1^{tm1Litt}$/J), CD11c.DOG,[33] RAG$^{-/-}$ (Rag1^{tm1Mom}), and RAG$^{-/-}$× CX_3CR1-GFP[5] were bred and kept under specific pathogen-free conditions in the animal facility of the Ulm University (Ulm, Germany). CX_3CR1-GFP animals were crossed with CD11c.DOG mice to obtain CX_3CR1-GFP×CD11c.DOG animals. Female and male mice were used at 6–12 weeks of age. All animal experiments were performed with groups of age- and sex-matched animals, and carried out according to the guidelines of the local Animal Use and Care Committee and the National Animal Welfare Law.

***C. rodentium* infection**. The strain *C. rodentium* ICC169 used in this study is a spontaneous nalidixic-acid-resistant mutant of the wt *C. rodentium* ICC168, which shows the same infectivity as the wt. RF-*C. rodentium* was generated by integrating the plasmid p16S_PT5mRuby into a 16S locus of the bacterial chromosome by homologous recombination (**Supplementary Figure S3** online). To construct p16S_mRuby, the vector p16Slux[28] was cut with *Pst*I to excise the *luxABCDE* genes and the P$_{help}$ promotor. The fragment encoding mRuby, including the upstream T5 promotor, was amplified from the plasmid pQE-32_mRuby[43] using KOD Hot Start DNA polymerase (Merck, Nottingham, UK) and primers PT5mRuby_ PstI.fwd (5′-AACTGCAGAGGCCCTTTCGTCTTCACC-3′) and PT5mRuby.rev (5′-GCTCAGCTAATTAAGCTTGGCTGC-3′). The PCR product was cut with *Pst*I and ligated to the p16S plasmid to yield p16S_mRuby. To generate RF-*C. rodentium*, the vector p16S_mRuby was transformed into *C. rodentium* ICC169 by electroporation, using standard protocols. Transformants were selected by plating cells on Luria–Bertani (LB) agar containing 300 μg ml^{-1} erythromycin, and resistant clones were tested for presence of p16S_mRuby by mini-prep and restriction analysis. Positive clones were incubated aerobically in LB broth containing erythromycin at 30 °C overnight, diluted 1:1,000 into fresh medium containing erythromycin, and incubated ~6 h at 30 °C. Thereafter, bacteria were incubated overnight at the nonpermissive temperature (42 °C). Dilutions were plated on LB agar containing erythromycin and incubated at 42 °C. Under these conditions, p16S_mRuby is unable to replicate due

◀

Figure 5 The depletion of $CX_3CR1^+CD11c^+$ macrophages results in an accelerated infection. (**a**) CX_3CR1-GFP animals were crossed with CD11c.DOG animals to obtain CX_3CR1-GFP×CD11c.DOG mice. CX_3CR1-GFP×CD11c.DOG mice were intraperitoneally injected with 30 ng bw g^{-1} diphtheria toxin (DT) every third day. Isolates were obtained from spleen, mesenteric lymph nodes (MLN), and colonic lamina propria (cLP), surface stained for CD11c, and analyzed by flow cytometry at the indicated time points. The numbers indicate the percentage of cells located in the respective area of the dot blots. (**b**) Colons were removed from nontreated and DT-treated CX_3CR1-GFP×CD11c.DOG animals, fixed in 4% paraformaldehyde sectioned on a microtome, mounted on slides, and analyzed by fluorescence microscopy Representative images from one individual mouse per group (from five individual mice per group analyzed) are shown. (**c**) Nontreated CD11c.DOG, DT-treated CD11c.DOG, $CX_3CR1^{GFP/+}$×CD11c.DOG, and $CX_3CR1^{GFP/GFP}$×CD11c.DOG were infected with 2×10^9 *Citrobacter rodentium.* Mean±s.e.m. loss of body weight (%) per group is shown for the indicated groups. In the nonparametric Student's *t*-test, $P<0.05$ was considered statistically significant (*$P<0.05$). (**d**) Survival of nontreated CD11c. DOG, DT-treated CD11c.DOG, $CX_3CR1^{GFP/+}$×CD11c.DOG, and $CX_3CR1^{GFP/GFP}$×CD11c.DOG infected with 2×10^9 *C. rodentium* is shown. At day 18 post infection, cLP cell isolates were obtained, stained for intracellular interleukin (IL)-22, and analyzed by flow cytometry. Numbers indicated the percentages of cells in the respective quadrants of the dot blots. (**e**) IL-22$^+$ cLP isolates from DT-treated CX_3CR1-GFP×CD11c.DOG animals were stained for CD3ε and CD4 at day 18 post infection and analyzed by multicolor flow cytometry. Numbers indicate the percentage of CD3ε$^+$, CD3ε$^+$CD4$^+$, CD4$^+$, and CD3ε$^-$CD4$^-$ cells within the IL-22$^+$ cell population. (**f**) Mean (±s.e.m.) percentage of IL-22$^+$ cells isolated from the cLP of nontreated CD11c.DOG and DT-treated (age- and sex-matched) $CX_3CR1^{GFP/+}$×CD11c.DOG and $CX_3CR1^{GFP/GFP}$×CD11c.DOG animals is shown. In the nonparametric Student's *t*-test, $P<0.05$ was considered statistically significant. (**g**) Mean (±s.e.m.) percentage of CD3ε$^-$CD4$^+$ lymphoid-tissue inducer cells within the IL22$^+$ cells from cLP isolates obtained from nontreated CD11c.DOG and DT-treated (age- and sex-matched) $CX_3CR1^{GFP/+}$× CD11c.DOG and $CX_3CR1^{GFP/GFP}$×CD11c.DOG animals is shown at day 18 post infection. P-values were calculated with a nonparametric Student's *t*-test; $P<0.05$ was considered statistically significant. (**h**) Mean±s.e.m. of colony forming units (CFUs) from plates spotted with homogenates from liver, spleen, and MLN of the indicated groups is presented. In the nonparametric Student's *t*-test, $P<0.05$ was considered statistically significant.

to the thermosensitive origin of replication, and thus is forced to integrate into a 16S locus of the bacterial chromosome by homologous recombination in the presence of selective concentrations of erythromycin. Erythromycin-resistant colonies were checked for red fluorescence, and the integration of p16S_PT5mRuby was confirmed by PCR. C. rodentium was prepared by culturing bacteria aerobically overnight in LB broth containing nalidixic acid (50 μg ml^{-1}) at 37 °C and centrifuged at 3,000 g for 10 min as previously reported.[11] RF-C. rodentium displayed identical infectivity as the parental wt strain C. rodentium ICC169, both in terms of bacteria recovered from the feces at all timepoints of infection and the clinical symptoms (data not shown). Pelleted bacteria were washed and resuspended in phosphate-buffered saline (PBS). Mice (6–12 weeks) were inoculated orally with 2×10^9 colony-forming units of either C. rodentium ICC169 (wt) or RF-C. rodentium. The weight of infected mice and their clinical condition were monitored every second day. Tissue samples were frozen in liquid nitrogen, cryosections were used and fixed in acetone at 4 °C for 30 min, mounted on slides, and stained with hematoxylin and eosin. Histology of the large intestine was categorized as for the severity of epithelial injury (graded 0–3, from absent to mild including superficial epithelial injury, moderate including focal erosions, and severe including multifocal erosions), the extent of inflammatory cell infiltrate (graded 0–3, from absent to transmural), and goblet cell depletion (0–3) as previously published.[44] In addition, the colon length and weight were determined, and colon weight/length ratios were calculated.

C. rodentium load in liver, spleen, MLNs, and feces. The organs were isolated aseptically from animals *post mortem*, and the organ weight was measured. The organs were then homogenized in sterile PBS. Serial dilutions of the homogenates were spotted on LB plates containing nalidixic acid (9 μg ml^{-1}) and nystatin (0.25 units ml^{-1}), incubated at 37 °C in a humidified atmosphere for 18 h, -forming units were counted, and bacterial load was calculated as cfu g^{-1} tissue. Similarly, fecal pellets were collected from each animal every 2–3 days over the course of the infection, weighted, and resuspended in 1 ml of PBS, plated in serial dilutions, and bacterial load was calculated as cfu g^{-1} feces.

Detection of anti-C. rodentium serum titers. Individual sera from littermate controls, heterozygous, or homozygous CX$_3$CR1-GFP mice were assayed for antigen-specific total IgG by enzyme-linked immunosorbent assay. Maxisorp immuno plates (catalog number (cat. no.) 442404; NUNC, Roskilde, Denmark) were coated with Gentamycin (10 μg ml^{-1})-treated bacteria (1×10^{10} colony-forming units per well) and incubated overnight at 4 °C. After being blocked and washed, the plates were incubated with diluted serum samples from infected and negative control from noninfected animals. Horseradish peroxidase-conjugated goat anti-mouse Ig (cat. no. 554002; BD Biosciences, Heidelberg, Germany) was used to detect binding of serum antibodies to C. rodentium epitopes. The reaction was developed and read at 492 nm on a Bio-TEK Synergy HT microplate-ELISA reader (Bio-TEK, Winooski, VT) using KC4 (v3.1) software (Bio-TEK, Bad Friedrichshall, Germany).

Confocal microscopy. The colon from noninfected and C. rodentium-infected CX$_3$CR1-GFP mice were opened by longitudinal incision and rinsed with PBS as previously described.[5] Living tissues were imaged with a LSM 710 confocal microscope (Zeiss, Jena, Germany). Colocalization analysis was carried out with the Zeiss ZEM software (Zeiss) by defining an area of interest and generating scatter diagrams. Image analysis was carried out with the LSM image browser (Zeiss) and Adobe Photoshop CS3.

Isolation of CX$_3$CR1$^+$ cells or of ILCs from the cLP. Segments of the colon were washed with PBS to remove debris and mucous. The epithelium was removed by incubation at 37 °C for 30 min under gentle shaking with 1 mM dithiothreitol and 1 mM EDTA in Ca^{2+}/Mg^{2+}-free PBS supplemented with 1% fetal calf serum. The remaining tissue was washed in PBS to remove residual epithelial cells, and the supernatants were discarded. Denuded tissues were cut into two to three 2-mm pieces

and digested with 0.5 mg ml^{-1} collagenase type VIII (cat. no. C-2139; Sigma-Aldrich, St Louis, MO) and 5 U ml^{-1} DNase (cat. no. 1284932; Roche, Basel, Switzerland) for 2 h at 37 °C in RPMI 1640/5% fetal calf serum. Supernatants were collected from which LP lymphocytes were pelleted. LP lymphocytes were resuspended in RPMI 1640 medium containing 40% Percoll (density 1.124 g dl^{-1}; cat. no. L-6145; Biochrome, Berlin, Germany). This cell suspension was overlaid onto 70% Percoll and centrifuged for 20 min at 750 g. Viable cells at the 40%/70% interface were collected and washed twice.

Flow cytometry analyses. Cells were washed twice in PBS/0.3% w/v bovine serum albumin supplemented with 0.1%w/v sodium azide. Nonspecific binding of antibodies to Fc receptors was blocked by pre-incubation of cells with monoclonal antibody (mAb) 2.4G2 (cat. no. 01241D; BD Biosciences) directed against the FcγRIII/II CD16/CD32 (1 μg/ml mAb per 10^6 cells). Cells were washed and incubated with 0.5 mg per 10^6 cells of the relevant mAb for 20 min at 4 °C and washed again twice. In most experiments, cells were subsequently incubated with a second-step reagent for 20 min at 4 °C. Four-color flow cytometry (FCM) analyses were performed using a FACSCalibur (BD Biosciences). The forward narrow-angle light scatter was used as an additional parameter to facilitate the exclusion of dead cells and aggregated cell clumps. Data were analyzed using FCS Express V3 software (De Novo Software, Los Angeles, CA).

Monoclonal antibodies. The following reagents and mAbs from eBioscience (Frankfurt, Germany) were used: antigen-presenting cell-conjugated mAb binding CD11c N418 (cat. no. 17-0114-82), anti-CD3 145-2C11 (cat. no. 553060), anti-CD25 PL61.5 (cat. no. 13-0251-81), and phycoerythrin-conjugated mAb-binding CD117 (c-Kit) 2B8 (cat. no. 12-1171-81). From BD Biosciences, the following biotinylated mAbs were used: anti–CD103 M290 (cat. no. 557493) and anti-CD3 145-2C11 (cat. no. 553060).

Intracellular cytokine staining. Cells (1×10^6 per ml) from MLN or cLP were stimulated for 4 h at 37 °C with 50 ng ml^{-1} PMA (cat. no. 79346; Sigma-Aldrich, St Louis, MO) and 500 ng ml^{-1} Ionomycin (cat. no. 10634; Sigma-Aldrich) in the presence of 10 μg ml^{-1} Brefeldin A (cat. no. ALX-350-019-M025; Alexis Biochemicals, Lörrach, Germany). Cells were harvested, washed, and stained with anti-CD3 145-2C11 (cat. no. 553060); eBioscience). Surface-stained cells were fixed (4% paraformaldehyde in PBS) and resuspended in permeabilization buffer (PBS, 0.5% bovine serum albumin, 0.5% saponin, 0.05% sodium azide). Permeabilized cells were incubated for 30 min at room temperature, dark with 0.25 μg/ml per 10^6 cells of the following antibodies: phycoerythrin-conjugated anti-IL-10 JES5-16E3 (cat. no. 12-7101-81; eBioscience), anti-RORγt AFKJS-9 (cat. no. 12-6988-82; eBioscience), anti-IL-22 (cat. no. IC582P; R&D, Wiesbaden, Germany), and anti-IL-12/IL-23p40 C17.8 (cat. no. 12-7123-81); antigen-presenting cell-conjugated anti-IL22 (cat. no. IL582A; R&D). Stained cells were washed twice in permeabilization buffer and resuspended in PBS supplemented with 0.3% w/v bovine serum albumin and 0.1% w/v sodium azide. The number of cytokine-expressing innate cells was determined by FCM.

Cytokine detection by quantitative real-time PCR. RNA was prepared from frozen colon tissue using the RNAeasy mini kit (cat. no. 74904; Qiagen, Hilden, Germany). Contaminating genomic DNA was eliminated from samples by treatment with RNAse-free DNAse I (cat. no. 1010395; Qiagen). A total of 2 μg of RNA isolated from tissue or 200 ng of RNA isolated from tissues was reverse transcribed with SuperScript II Reverse Transcriptase (cat. no. 18064-014; Invitrogen, Paisley, Scotland) using random primers (cat. no. 48190-011; Invitrogen) according to the manufacturer's instructions. SYBR Green qPCR Master mix (cat. no. PA-012-12; SABiosciences, Valencia, CA) was used for amplification and detection. Real-time PCR reactions were performed using the 7500 Fast Real-Time PCR System (Applied Biosystems, Darmstadt, Germany) and the following conditions: 50 °C for 2 min, repeat 1; 95 °C for 10 min, repeat 1; 95 °C

for 15 s, 60 °C for 1 min, repeats 40; 95 °C for 15 s, 60 °C for 1 min, 95 °C for 15 s, 60 °C for 15 s, repeat 1. β-actin PCR signals were used to equalize cDNA amounts between preparations. Following primers were used: β-actin (cat. no. PPM02945A; SABiosciences); *REG IIIγ* (cat. no. QT00147455; Qiagen); *REG III*β (cat. no. QT00239302; Qiagen); *Cx₃cl1* (cat. no. PPM0959E; SABiosciences); *IL-1*β ((forward) 5′-CTC AAT GGA CAG AAT ATC AAC CAA CA)-3′; IL-22 (cat. no. PPM05481A; Qiagen), *IL-12p40* ((forward) 5′-ACT TGA AGT TCA ACA TCA AGA GCA GTA G-3′); *IL-12p19* (IL23a) (cat. no. QT01663613; Qiagen). Expected product length: 154 bp for β-*actin*, 93 bp for *REG IIIγ*, 141 bp for *REG III*β, 113 bp for *Cx₃cl1*, 28 bp for *IL-12p40*, 80 bp *IL-12p19*, 99 bp for IL-22, and 26 bp for *IL-1*β. β-*actin* PCR signals were used to equalize cDNA amounts between preparations.

Statistics. A one-way ANOVA test (for nonparametric) data and a *t*-test for two unequal variances were used. $P < 0.05$ was considered statistically significant.

DISCLOSURE
The authors declared no conflict of interest.

REFERENCES
1. Strober, W. The multifaceted influence of the mucosal microflora on mucosal dendritic cell responses. *Immunity* **31,** 377–388 (2009).
2. Khor, B., Gardet, A. & Xavier, R.J. Genetics and pathogenesis of inflammatory bowel disease. *Nature* **474,** 307–317 (2011).
3. Maloy, K.J. & Powrie, F. Intestinal homeostasis and its breakdown in inflammatory bowel disease. *Nature* **474,** 298–306 (2011).
4. Hadis, U. *et al.* Intestinal tolerance requires gut homing and expansion of FoxP3+ regulatory T cells in the lamina propria. *Immunity* **34,** 237–246 (2011).
5. Niess, J.H. & Adler, G. Enteric flora expands gut lamina propria CX3CR1+ dendritic cells supporting inflammatory immune responses under normal and inflammatory conditions. *J. Immunol.* **184,** 2026–2037 (2010).
6. Rivollier, A., He, J., Kole, A., Valatas, V. & Kelsall, B.L. Inflammation switches the differentiation program of Ly6Chi monocytes from antiinflammatory macrophages to inflammatory dendritic cells in the colon. *J. Exp. Med.* **209,** 139–155 (2012).
7. Kayama, H. *et al.* Intestinal CX3C chemokine receptor 1high (CX3CR1high) myeloid cells prevent T-cell-dependent colitis. *Proc. Natl Acad. Sci. USA* **109,** 5010–5015 (2012).
8. Niess, J.H. *et al.* CX3CR1-mediated dendritic cell access to the intestinal lumen and bacterial clearance. *Science* **307,** 254–258 (2005).
9. Ishida, Y. *et al.* Essential involvement of CX3CR1-mediated signals in the bactericidal host defense during septic peritonitis. *J. Immunol.* **181,** 4208–4218 (2008).
10. Mundy, R., MacDonald, T.T., Dougan, G., Frankel, G. & Wiles, S. Citrobacter rodentium of mice and man. *Cell Microbiol.* **7,** 1697–1706 (2005).
11. Symonds, E.L. *et al.* Involvement of T helper type 17 and regulatory T cell activity in Citrobacter rodentium invasion and inflammatory damage. *Clin. Exp. Immunol.* **157,** 148–154 (2009).
12. Borenshtein, D., McBee, M.E. & Schauer, D.B. Utility of the Citrobacter rodentium infection model in laboratory mice. *Curr. Opin. Gastroenterol.* **24,** 32–37 (2008).
13. Eckmann, L. Animal models of inflammatory bowel disease: lessons from enteric infections. *Ann. NY Acad. Sci.* **1072,** 28–38 (2006).
14. Aujla, S.J. *et al.* IL-22 mediates mucosal host defense against Gram-negative bacterial pneumonia. *Nat. Med.* **14,** 275–281 (2008).
15. Wolk, K. *et al.* IL-22 increases the innate immunity of tissues. *Immunity* **21,** 241–254 (2004).
16. Harper, E.G. *et al.* Th17 cytokines stimulate CCL20 expression in keratinocytes *in vitro* and *in vivo*: implications for psoriasis pathogenesis. *J. Invest Dermatol.* **129,** 2175–2183 (2009).
17. Liang, S.C. *et al.* IL-22 induces an acute-phase response. *J. Immunol.* **185,** 5531–5538 (2010).
18. Guilloteau, K. *et al.* Skin inflammation induced by the synergistic action of IL-17A, IL-22, Oncostatin M, IL-1{alpha}, and TNF-{alpha} recapitulates some features of psoriasis. *J. Immunol.* **184,** 5263–5270 (2010).
19. Sonnenberg, G.F., Monticelli, L.A., Elloso, M.M., Fouser, L.A. & Artis, D. CD4(+) lymphoid tissue-inducer cells promote innate immunity in the gut. *Immunity* **34,** 122–134 (2011).
20. Mangan, P.R. *et al.* Transforming growth factor-beta induces development of the T(H)17 lineage. *Nature* **441,** 231–234 (2006).
21. Cella, M. *et al.* A human natural killer cell subset provides an innate source of IL-22 for mucosal immunity. *Nature* **457,** 722–725 (2009).
22. Spits, H. & Di Santo, J.P. The expanding family of innate lymphoid cells: regulators and effectors of immunity and tissue remodeling. *Nat. Immunol.* **12,** 21–27 (2011).
23. Spits, H. Another armament in gut immunity: lymphotoxin-mediated crosstalk between innate lymphoid and dendritic cells. *Cell Host Microbe* **10,** 3–4 (2011).
24. Tumanov, A.V. *et al.* Lymphotoxin controls the IL-22 protection pathway in gut innate lymphoid cells during mucosal pathogen challenge. *Cell Host Microbe* **10,** 44–53 (2011).
25. Sawa, S. *et al.* RORgammat+ innate lymphoid cells regulate intestinal homeostasis by integrating negative signals from the symbiotic microbiota. *Nat. Immunol.* **12,** 320–326 (2011).
26. Arques, J.L. *et al.* Salmonella induces flagellin- and MyD88-dependent migration of bacteria-capturing dendritic cells into the gut lumen. *Gastroenterology* **137,** 579–587 (2009).
27. Jung, S. *et al.* Analysis of fractalkine receptor CX(3)CR1 function by targeted deletion and green fluorescent protein reporter gene insertion. *Mol. Cell Biol.* **20,** 4106–4114 (2000).
28. Riedel, C.U. *et al.* Construction of p16Slux, a novel vector for improved bioluminescent labeling of gram-negative bacteria. *Appl. Environ. Microbiol.* **73,** 7092–7095 (2007).
29. Zheng, Y. *et al.* Interleukin-22 mediates early host defense against attaching and effacing bacterial pathogens. *Nat. Med.* **14,** 282–289 (2008).
30. Ota, N. *et al.* IL-22 bridges the lymphotoxin pathway with the maintenance of colonic lymphoid structures during infection with Citrobacter rodentium. *Nat. Immunol.* **12,** 941–948 (2011).
31. Wehkamp, J., Schauber, J. & Stange, E.F. Defensins and cathelicidins in gastrointestinal infections. *Curr. Opin. Gastroenterol.* **23,** 32–38 (2007).
32. Simmons, C.P. *et al.* Central role for B lymphocytes and CD4+ T cells in immunity to infection by the attaching and effacing pathogen Citrobacter rodentium. *Infect. Immun.* **71,** 5077–5086 (2003).
33. Hochweller, K., Striegler, J., Hammerling, G.J. & Garbi, N. A novel CD11c. DTR transgenic mouse for depletion of dendritic cells reveals their requirement for homeostatic proliferation of natural killer cells. *Eur. J. Immunol.* **38,** 2776–2783 (2008).
34. Dahan, S. *et al.* EspJ is a prophage-carried type III effector protein of attaching and effacing pathogens that modulates infection dynamics. *Infect. Immun.* **73,** 679–686 (2005).
35. Brand, S. *et al.* Increased expression of the chemokine fractalkine in Crohn's disease and association of the fractalkine receptor T280M polymorphism with a fibrostenosing disease Phenotype. *Am. J. Gastroenterol.* **101,** 99–106 (2006).
36. Sugimoto, K. *et al.* IL-22 ameliorates intestinal inflammation in a mouse model of ulcerative colitis. *J. Clin. Invest.* **118,** 534–544 (2008).
37. Brand, S. *et al.* IL-22 is increased in active Crohn's disease and promotes proinflammatory gene expression and intestinal epithelial cell migration. *Am. J. Physiol. Gastrointest. Liver Physiol.* **290,** G827–G838 (2006).

38. Mizutani, N. *et al.* Dose-dependent differential regulation of cytokine secretion from macrophages by fractalkine. *J. Immunol.* **179,** 7478–7487 (2007).

39. Inui, M. *et al.* Protective roles of CX3CR1-mediated signals in toxin A-induced enteritis through the induction of heme oxygenase-1 expression. *J. Immunol.* **186,** 423–431 (2011).

40. Fogg, D.K. *et al.* A clonogenic bone marrow progenitor specific for macrophages and dendritic cells. *Science* **311,** 83–87 (2006).

41. Geissmann, F., Jung, S. & Littman, D.R. Blood monocytes consist of two principal subsets with distinct migratory properties. *Immunity* **19,** 71–82 (2003).

42. Brand, S., Sakaguchi, T., Gu, X., Colgan, S.P. & Reinecker, H.C. Fractalkine-mediated signals regulate cell-survival and immune-modulatory responses in intestinal epithelial cells. *Gastroenterology* **122,** 166–177 (2002).

43. Kredel, S. *et al.* mRuby, a bright monomeric red fluorescent protein for labeling of subcellular structures. *PLoS One* **4,** e4391 (2009).

44. Conlin, V.S. *et al.* Vasoactive intestinal peptide ameliorates intestinal barrier disruption associated with Citrobacter rodentium-induced colitis. *Am. J. Physiol. Gastrointest. Liver Physiol.* **297,** G735–G750 (2009).